I²MTC 2008 – IEEE International Instrumentation and
Measurement Technology Conference
Victoria, Vancouver Island, Canada, May 12–15, 2008

A Simple, Low Cost, 3D Scanning System Using the Laser Light-Sectioning Method

Beverly D. Bradley[1], Adrian D.C. Chan[1], M. John D. Hayes[2]
[1]Systems and Computer Engineering, Carleton University
[2]Mechanical and Aerospace Engineering, Carleton University
1125 Colonel By Drive, Ottawa, Ontario, Canada K1S 5B6

Abstract *– The use of 3D scanning systems for acquiring the external shape features of arbitrary objects has many applications in industry, computer graphics, and more recently, the biomedical field. The potential exists to expand the use of 3D models even further, by continuing to develop simpler, more cost effective systems. A simple, lost cost, 3D scanning system is presented which employs a laser light-sectioning technique. Results of a proof of concept experiment for the proposed system demonstrate the validity of the chosen approach. Directions for future work are also discussed.*

Keywords *– 3D geometric modeling, 3D scanning, laser light-sectioning, reverse engineering*

I. INTRODUCTION

For many years, three-dimensional (3D) scanning has been widely used for industrial applications such as reverse engineering and part inspection [1]. Over the past few years, dramatic decreases in the cost of 3D scanning equipment has led to its increased use for many other applications, including rapid prototyping and modeling, development of realistic computer graphics in the video gaming market [1], and more recently, in the biomedical field for applications such as anatomical parts reconstruction [2], orthodontic treatment planning [3], cranial deformation research [4], and cartilage morphology studies [5]. The potential exists to expand the use of 3D models even further, by continuing to develop simpler, more cost effective systems for acquiring external shape features of arbitrary objects.

There exists a variety of different techniques for acquiring 3D models of objects, all with a wide range of hardware costs, and differing levels of achievable accuracy and detail in the captured geometric models. Streaming video and image-based techniques, structured light and laser light-sectioning methods, time-of-flight range finders, shape-from-silhouette algorithms and space carving techniques, are all methods which have been studied in recent years. A good review of 3D model acquisition techniques and the processing of range scanner output data into efficient numerical representations of objects can be found in [1].

Although the current state of the art allows for the acquisition of a large class of objects, expert operators and time consuming procedures are required for all but the simplest cases [1]. Hence, several key areas of research for the improvement of the 3D model acquisition pipeline have been identified in [1] as follows:

1. planning methods for data acquisition;
2. reliable capture and robust processing of data for a larger class of objects, environments, and objects with challenging surface properties;
3. automation of all the steps, to minimize user input;
4. real-time feedback of the acquired surface;
5. improved capture and representation of surface appearance; and
6. methods for assessing global model accuracy after range scan registration.

We are looking for a simple 3D scanning system which will attempt to address points 2, 3 and 6, with the underlying goals of being cost effective and versatile. We have decided to focus upon the laser light-sectioning method, an accepted technique for measuring the 3D shape of a target object. The technique involves measuring the position of an object's surface profile by recording where the profile intersects a laser light plane. Currently available commercial 3D scanning systems employing this technique have been found to cost anywhere from $2,500 to $240,000 USD. The most economical of these found to date is developed by NextEngine (Santa Monica, California). Their *Desktop 3D Scanner* system, designed for small to medium sized objects, uses proprietary Multi-stripe Laser Triangulation [6]. Their system sells for $2,500 USD and offers an accuracy of ±0.38mm. The accompanying software for the scanner costs an additional $1,000 to $2,500 USD.

A key feature of the proposed system will be the ability of the camera system to rotate about an object with the required number of degrees of freedom making it flexible for numerous applications; particularly for biomedical applications where the apparatus would ideally rotate about a patient and not vice versa.

In Section II, a general system overview of the laser light-sectioning method is presented, followed by a description of the proposed system and methodology in Section III. The results of a proof of concept experiment using this proposed approach are presented in Section IV. Section V and VI include a discussion with points for future work and conclusions, respectively.

II. GENERAL SYSTEM OVERVIEW

This section describes a general system for obtaining a 360° model of the external profile of an object via laser light-sectioning.

A. General System Setup and Data Acquisition Process

A typical system employing this technique would have the following setup (Fig. 1). A laser diode fitted with line optics creates a horizontal light plane (i.e. parallel to the xy-plane), the trace of which is visible when projected onto the object of interest. The image of this trace is recorded with a CCD camera, which is inclined at a fixed angle α, relative to the xy-plane. The goal of each measurement is to obtain one segment of one planar section of the object [7].

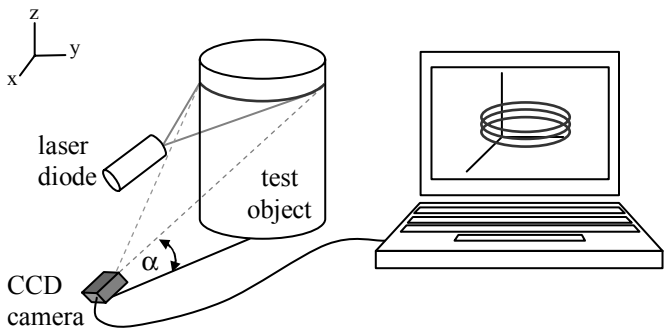

Fig. 1. Laser light-sectioning system diagram

With this setup, a scaled reconstruction of the exterior features of an object can be created. A single planar section of the object is constructed by: a) capturing M views of the laser trace in the plane of the section, separated by rotations of R=360°/M about the vertical z-axis; b) transforming the laser trace segments using a transformation obtained from a calibration procedure to remove the projective distortion of the camera; and c) rectifying the laser trace segments to form an entire 360° outline of the external profile features of the object. Repeating this process for N planar cross-sections in the z-axis and stacking them along the vertical axis results in a 3D wire frame outline of the object.

B. General Data Processing Steps

The general data processing steps are outlined in the flow diagram in Fig. 2 and described in sequence below.

Image Processing. First, for the image processing stage, the laser trace images acquired would undergo preprocessing in order to condition the images for effective thresholding. This could involve background removal techniques or contrast adjustments. Then the image is thresholded to isolate the laser trace from the rest of the image. The last step of the image processing stage involves determining a discrete set of point coordinates to represent the laser trace. This could be accomplished with line thinning algorithms [8], [9], center of gravity techniques [10], or line walking algorithms [10]. The laser trace images can then be manipulated for reconstruction.

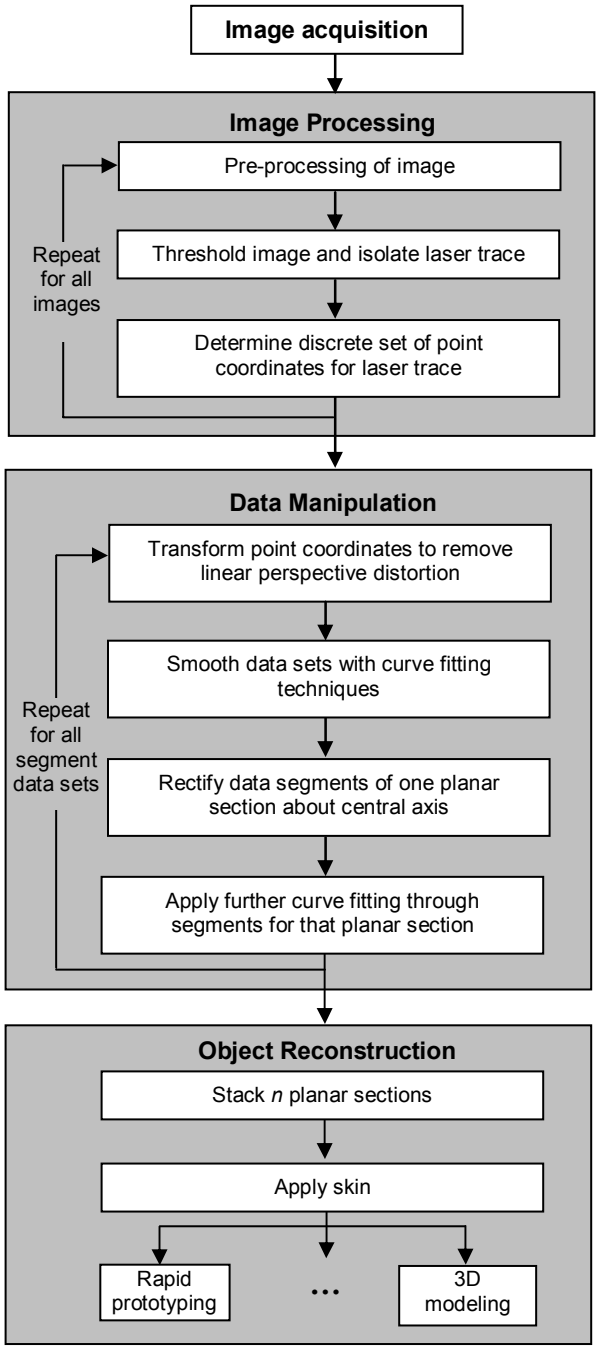

Fig. 2. Flow diagram of general data processing steps for the laser light-sectioning technique

Data manipulation. A transformation matrix is used to transform the sets of point coordinates, removing the linear portion of the projective distortion; the transformation matrix can be determined by imaging a calibration grid. Depending on the algorithm used for determining the point coordinates,

the data segments may be quite noisy and can be smoothed with curve fitting techniques before proceeding. For a given plane, the *M* segments of point coordinates are then rotated according to their angular position about the central axis of rotation. With the full object contour of a single planar section now in place, further curve fitting techniques can be applied through these segments to define a smooth continuous curve.

Object Reconstruction. Planar sections are stacked along the central axis of rotation. Once this wire frame is constructed, a skin can be fit to these outlines using triangle mesh techniques [11], non-uniform rational B-splines (NURBS) [12], or other methods [13]. The resultant 3D model can then be used for any number of applications, including reverse engineering, 3D printing or rapid prototyping, and 3D computer modeling for industrial or biomedical purposes.

III. PROPOSED APPROACH

This section outlines the system implemented to carry out the general process, described in Section II.

A. System Setup and Data Acquisition Process

The current system consists of a TM-200 High Resolution CCD camera and a Lasiris Diode Laser. Both are mounted to a fixed stand; the camera is inclined at $\alpha = 40°$. Images are captured with a NI PCI-1411 image acquisition device. The estimated cost of the system is approximately $2,500 CDN.

A calibration grid of known dimensions was used to calibrate the measurement head. Since all recorded laser traces lie in the laser plane, images can be calibrated by superimposing the plane of the calibration grid on this laser plane and recording an image. A homogeneous transformation matrix, *T*, is computed which maps points in the image plane of the camera to their corresponding points on the known calibration grid, thereby eliminating the linear portion of the projective distortion [7]. The geometry can be represented by the linear transformation presented in (1).

$$\rho \begin{bmatrix} W_0 \\ W_1 \\ W_2 \end{bmatrix} = \begin{bmatrix} t_{11} & t_{12} & t_{13} \\ t_{21} & t_{22} & t_{23} \\ t_{31} & t_{32} & t_{33} \end{bmatrix} \begin{bmatrix} w_0 \\ w_1 \\ w_2 \end{bmatrix} \quad (1)$$

or, more compactly,

$$\rho W = Tw, \quad (2)$$

where $W = (W_0, W_1, W_2)$ are the coordinates of a point in the image plane, $w = (w_0, w_1, w_2)$ are the coordinates of the same point on the calibration grid, and ρ represents a scaling factor which, when factored out, leaves the point *W* that corresponds to a point in a Cartesian coordinate system (even though the mapping is projective).

Coordinates of 4 known points, along with those of their corresponding images, are enough to uniquely identify the 8 independent elements of the transformation matrix *T,* and the independent scaling factor ρ. Only the elements of *T* are required to transform all other image points from the projective into the Cartesian plane. For the results presented here, this was the approach used to compute *T*. A second technique involving a least squares minimization approach was also explored and is further discussed in Section V.

As part of the calibration procedure, a scaling factor must be determined; this can be done using a calibration object of a known size. In this experiment, a calibration cylinder with diameter 28.58 mm (1⅛ in) was used. $M = 8$ images of the laser trace on the calibration cylinder were captured in rotational increments of $R = 45°$. The system to rotate the measurement head is still under development, necessitating manual manipulation for these preliminary experiments. Rather than manually rotate the measurement head, the equivalent problem was to rotate the object of interest. Fig. 3 shows an image of the cylinder in the test jig as well as a raw image of a laser plane intersecting the cylinder with appropriate lighting for visualizing the laser trace.

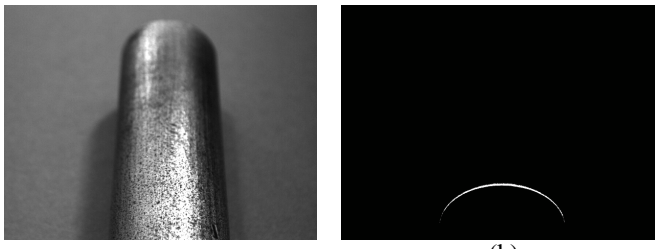

(a) (b)

Fig. 3. (a) Cylinder in test jig and (b) laser trace on cylinder

Once the images of the calibration cylinder were taken, images for $N = 4$ planar sections of a simple test object were captured to demonstrate the validity of our approach; this test object was a cylinder with diameter 19.05 mm (¾ in). For each plane, as was done for the calibration cylinder, $M = 8$ images of the laser trace on the object were captured in rotational increments of $R = 45°$. Planar sections were captured at 3.175 mm (⅛ in) increments in the negative z-axis direction. To accomplish this, the object was raised with respect to the laser plane using 3.175 mm (⅛ in) gauge blocks. In total, 32 images of laser trace segments were captured for reconstructing the 4 planar sections.

B. Data Processing Steps

According to Fig. 2, the data processing steps implemented were as follows:

Image Processing. Using Matlab, a simple background eliminating algorithm was applied to the images, before thresholding, to isolate the laser line traces. Next, a discrete set of point coordinates for each laser trace segment, representing the best path through the raw image, was

determined using an iterative thinning algorithm available in Matlab [8], which thinned the segments to 8-connected skeletons, retaining diagonal lines and 2×2 squares according to [9].

Data manipulation. The set of point coordinates for each segment was mapped to the Cartesian plane using the transformation matrix *T* obtained from the camera calibration procedure. The end regions of the data segments were plagued with noise, excessively steep slopes, and frequent outliers. This is due to the poor quality of the light signal where it intersects the outermost edges of the object [7]. For this reason, the first and last 10% of data points were discarded for the remainder of the analysis. A polynomial was then fit to each of the truncated arc segments to smooth out the data.

The 8 segments were then reassembled into planar sections. A suitable longitudinal axis, upon which the segments could be reassembled, was determined using the calibration cylinder. Using an improved version of the algorithm found in [14], the centres of the transformed and fitted arcs of the calibration cylinder were determined. Then, using the arc centre coordinates as a reference frame origin, coordinates of the test object segments were translated accordingly, and rotated to their respective rotation angle.

For the final curve fitting step of the data manipulation stage, Elliptical Fourier Descriptors (EFDs) [15] were used to fit a smooth curve through the segments of each planar section. A 2D continuous closed contour can be represented parametrically as a function of time, *V(t)*; projections of this vector function on the x and y axis, represented by *x(t)* and *y(t),* are periodic with period *P,* where *P* is the time required to trace the entire contour at a constant speed. These projections can be represented by Fourier trigonometric series, the coefficients of which are referred to as EFDs. Different levels of approximation to the closed contour represented by *x(t)* and *y(t)* can be obtained by truncating the Fourier series after different numbers of harmonics [16]. In this case, only 1 harmonic was required to fit the calibration cylinder; however, higher order harmonics could be used to fit more complicated object profiles. Further work is required to develop a preprocessing technique that would identify an appropriate number of harmonics to use for a given set of data segments, since not all objects imaged would have circular symmetry as in this test case. While EFDs are particularly suitable for representing most biological objects [17], other methods are also being investigated to account for cases where discontinuities in the laser trace exist (e.g. sharp edges).

Object Reconstruction. The final object contours were appropriately stacked along the reconstruction z-axis.

IV. RESULTS

Fig. 4 shows a planar section of the calibration cylinder scaled according to the known diameter of the cylinder, 28.58 mm (1 ⅛ in). Solid arcs represent the 8 original data segments and the dashed line indicates the first harmonic EFD fit. To visibly distinguish overlapping arcs, different line thicknesses and shades are used. Segments 1 to 4 alternate from light to dark, and decrease in thickness; this pattern repeats for segments 5 to 8 such that opposing arcs are represented with the same line type. The beginning of segment 1 is indicated and subsequent segments are numbered counterclockwise. Fig. 5 shows the four planar sections of the test cylinder scaled according to the scaling factor obtained from the calibration cylinder.

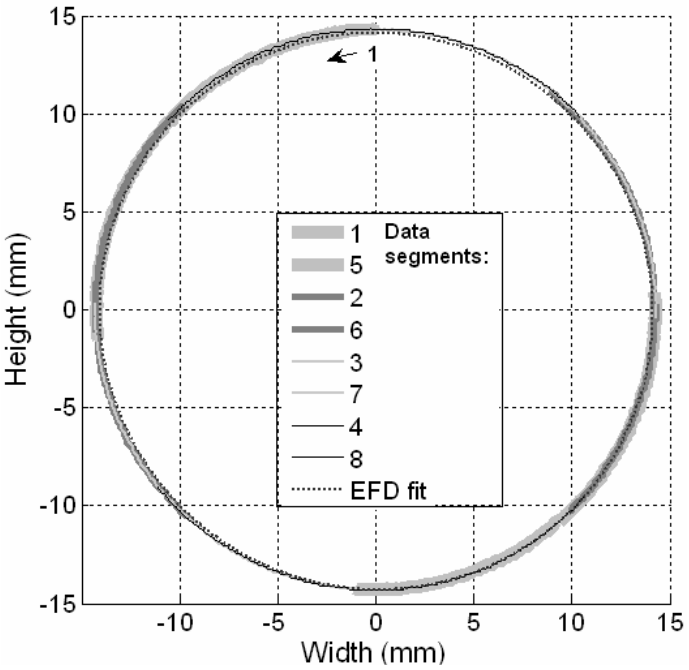

Fig. 4. Reconstructed planar section of calibration cylinder

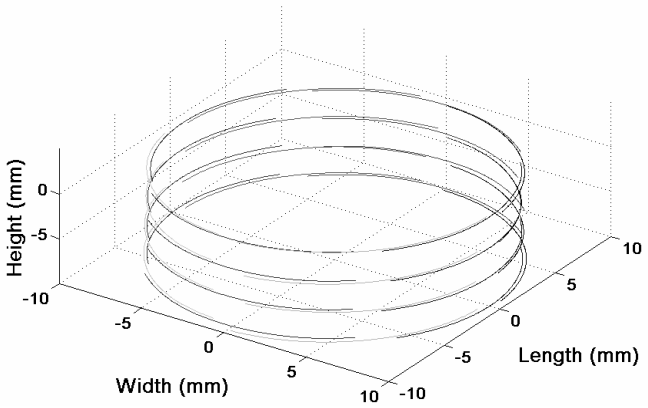

Fig. 5. Four reconstructed planar sections of a test cylinder

V. DISCUSSION & FUTURE WORK

As shown in Fig. 4, the rectified segments for the planar section of the calibration cylinder appear to produce a fairly good result, even before the data were fitted with the EFD

technique. The polynomial curve fitting applied to the arcs has produced segments that fit quite seamlessly together. The subsequent EFD fit through the segments does however indicate that an ideal circle was not obtained.

Visual inspection of the reconstructed planar sections of the test cylinder (Fig. 5) reveals that the procedure developed can produce a wire-frame model, which is reasonably complete in desired external detail. The application of a mesh skin has yet to be implemented. There are visible errors where the data segments overlap that must be reconciled. The most prominent sources of this error for this setup were procedural in nature and include: misalignment of the test object after manually raising it with the gauge blocks, and inaccuracies associated with manually turning the object in its place. These errors are associated with limitations of the current setup, and will be attenuated or eliminated with future versions of the prototype in which the camera and laser diode head will be precisely manipulated about the object in an automated manner. The center of rotation can also be guaranteed with much better precision than manually rotating the object. With these errors attenuated, efforts can be focused on eliminating other systematic and random errors. Despite the fact that manual manipulation was used to acquire the data, the percent error between the diameter of the reconstructed object and the actual diameter of the object is about 0.67%, which translates to an error of less than 0.5 mm.

An anticipated systemic error would be inaccuracy of the image calibration process. The current calibration procedure could be improved by refining the process for acquiring grid intersection points of the calibration image down to sub-pixel accuracy using better line-walking algorithms. As mentioned in Section III, another approach for finding the transformation matrix was implemented using a least-squares approach, whereby an optimal T was found by minimizing an error criteria function. In this case, additional pairs of matching points can be used to find the least-squares estimate of the 9 parameters of the transformation that best maps the given set of image points to their matching point pairs on the calibration grid. This approach would be beneficial for coping with noise that may be associated with acquiring grid point locations for the control point pairs. Due to the projective nature of the transformation, however, the direct linear transformation (DLT) algorithm for determining homographic transformations needs to be investigated in more depth. In either case, further investigation of how *both* methods perform under noisy conditions would be beneficial. Under the current test conditions, the difference between the method used (as described in Section III) and the least-squares estimate was found to be negligible.

A random error would be error due to noise in the measurements themselves. To deal with error associated with the point coordinates found for the data segments, polynomial curve fits were implemented; however, a further approach to deal with this error, as suggested in [1], would be to redefine the point coordinates in those regions where segments overlap by averaging samples from those overlapping scans. Also, during image acquisition, reducing the angle increment and taking more image samples would result in greater overlap between segments and would allow for the truncation of more than 10% of the data (as was done here), further eliminating the occurrence of outliers and end effects in those inherently noisy regions. The tradeoff of course is an increased acquisition time.

Also, as was mentioned, the use of EFDs could be extended to involve preprocessing to determine the most appropriate number of harmonics for a given set of segments, resulting in accurate contour fitting without excessive data processing.

VI. CONCLUSION

There is good reason to believe that an acceptable level of accuracy can be achieved in future iterations of the design. Sub-mm accuracy has already been achieved with the current setup, where the majority of the errors are the result of manual manipulation of the device, which is going to be addressed in the next iteration of the prototype. Since the data are, as yet, too noisy to obtain satisfactory dimensional tolerance, no precise value can be assigned to the system's dimensional accuracy. The overall cost of the system's components is well below the least expensive system found on the market when the price of software is considered. With the overall goals of this project being to develop a robust, simple, cost effective, and flexible 3D modeling apparatus that can be used for a variety of different applications, the results presented here show considerable progress towards these objectives.

ACKNOWLEDGMENT

This work was supported in part by a grant from the National Science and Engineering Research Council (NSERC). Paul O`Leary (Institute for Automation, University of Leoben, Leoben, Austria) and M. John D. Hayes (Mechanical and Aerospace Engineering, Carleton University) are acknowledged for the partial use of their Matlab code for some of the data processing steps.

REFERENES

[1] F. Bernardini and H. Rushmeier, "The 3D model acquisition pipeline," *Computer Graphics Forum,* vol.21, no.2, pp.149-172, 2002.

[2] G. Tognola, M. Parazzini, P. Ravazzani, F. Grandori, and C. Svelto, "3D Acquisition and quantitative measurements of anatomical parts by optical scanning and image reconstruction from unorganized range data", *IEEE Trans. Instrum. Meas.,* vol. 52, no. 5, pp. 1665-1673, Oct. 2003.

[3] M.Y. Hajeer, D.T. Millett, A.F. Ayoub, and J.P. Siebert, "Applications of 3D imaging in orthodontics: Part I," *J. of Orthodontics*, vol.31, pp.62–70, 2004.

[4] R.J. Hennessy, S. McLearie, and A. Kinsella, "Facial surface analysis by 3D laser scanning and geometric morphometrics in relation to sexual dimorphism in cerebral–craniofacial morphogenesis and cognitive function," *J. of Anatomy*, vol.207, pp.283–295, 2005.

[5] N.H. Trinh, J. Lester, B.C. Fleming, G. Tung, and B.B. Kimia, "Accurate measurement of cartilage morphology using a 3D laser scanner," in *Proc. of 2nd Int'l ECCV Workshop on Computer Vision Approaches to Medical Image Analysis (CVAMIA '06*), Graz, Austria, pp.37-48, May 2006.

[6] J.A. Jalkio, R.C. Kim, S.K. Case, "Three dimensional inspection using multistripe structured light", *Optical Engineering,* vol.24, pp. 966-974, 1985.

[7] M.J.D. Hayes, M. Leitner, P. O'Leary, R. Ofner, and C. Sallinger, "An integrated optical-robotic measurement system," in *Proc. 8th Canadian Congress of Applied Mechanics (CANCAM '01),* St. John's, Nfld., Canada, pp.287-288, 2001.

[8] L. Lam, S-W. Lee, and C.Y. Suen, "Thinning methodologies – A comprehensive survey," *IEEE Trans. Pattern Analysis & Machine Intelligence,* vol.14, no.9, pp.869-885, Sept. 1992.

[9] Z. Guo and R.W. Hall, "Parallel thinning with two-subiteration algorithms," *Comm. ACM,* vol.32, no.3, pp. 359-373, 1989.

[10] R. Ofner, P. O'Leary, and M. Leitner, "A collection of algorithms for the determination of construction points in the measurement of 3D geometries via light-sectioning," *2nd Workshop on European Scientific and Industrial Collaboration promoting: Advanced Technologies in Manufacturing (WESIC '99),* Newport, South Wales, U.K., pp.505-512, 1999.

[11] C.L. Bajaj, E. J. Coyle, and K-N. Lin, "Surface and 3D Triangular Meshes from Planar Cross Sections," *5th International Meshing Roundtable*, Sandia National Laboratories, pp.169-178, October 1996.

[12] L. Piegl, "On NURBS: A survey," *IEEE Computer Graphics and Applications,* vol.11, no.1, pp.55-71, 1991.

[13] R.M. Bolle and B.C. Vemuri, "On Three-dimensional surface reconstruction methods," *IEEE Trans. Pattern Analysis and Machine Intelligence,* vol.13, no.1, pp.1-13, 1991.

[14] Z. Wu, L. Wu, and A. Wu, "The robust algorithms for finding the center of an arc," *Computer Vision and Image Understanding,* vol.62, no.3, pp. 269-278, 1995.

[15] F.P. Khul and C.R. Giardina, "Elliptic Fourier features of a closed contour," *Computer Graphics and Image Processing,* vol.18, pp.236-258, 1982.

[16] R. Safaee-Rad, K.C. Smith, B. Benhabib, and I. Tchoukanov, "Application of moment and Fourier descriptors to the accurate estimation of elliptical shape parameters," *Proc. Int'l Conf. Acoustics, Speech and Signal Processing (ICASSP '91),* April 1991, pp.2465 – 2468.

[17] Y. Jeong and R.J. Radke, "Reslicing axially sampled 3D shapes using elliptic Fourier descriptors," *Medical Image Analysis,* vol.11, pp.197-206, 2007.